SYNTHESIS AND CHARACTERIZATION
OF HYDROXYAPATITE/CHITOSAN COMPOSITES

Tomasz SZATKOWSKI[*], **Agnieszka KOŁODZIEJCZAK-RADZIMSKA**[*],
Jakub ZDARTA[*], **Karolina SZWARC-RZEPKA**[*], **Dominik PAUKSZTA**[*],
Marcin WYSOKOWSKI[*], **Hermann EHRLICH**[**], **Teofil JESIONOWSKI**[*]

[*]   Poznan University of Technology, Faculty of Chemical Technology, Institute of Chemical Technology and
Engineering, M. Sklodowskiej–Curie 2, PL-60965, Poznan, Poland, teofil.jesionowski@put.poznan.pl
[**]   TU Bergakademie Freiberg, Institute of Experimental Physics, Biomineralogy and Extreme Biomimetics
Group, Leipziger Str. 23, 09599 Freiberg, Germany

Abstract: Hydroxyapatite (HAp)/chitosan (CS) composites were synthesized via a one-step co-precipitation method from aqueous solution, with the use of calcium chloride ($CaCl_2$) and disodium hydrogen phosphate (Na_2HPO_4). CS was obtained via partial deacetylation of chitin with the use of strong sodium hydroxide solution. Composites were prepared with various HAp/CS ratios (30/70, 50/50, 70/30, 85/15) for comprehensive comparison of their properties. Fourier Transform Infrared Spectroscopy (FT-IR) analysis showed that hydrogen bonds were formed between the organic matrix and the mineral compound, confirming a successful phase interconnection. X-ray diffraction patterns were obtained, enabling examination of the crystalline properties of the composites, including HAp identification. The porous structure parameters of the composites were investigated, and morphological analysis (SEM) was performed. Differential Thermal Gravimetry (DTG) analysis of the composites indicated that the material is thermally stable up to 200 °C. Additionally, Energy Dispersive Spectroscopy (EDS) analysis of the mineral was carried out to check the Ca/P ratio, and confirmed its similarity to pure HAp.

Keywords: hydroxyapatite, chitosan, composite, one-step co-precipitation

Introduction

Biomaterials have recently received greater widespread attention due to their increasing value in the treatment of damaged mammalian tissue, most importantly in the human body. Synthetic, inorganic materials based on calcium phosphate, in particular tricalcium phosphate (TCP, $Ca_3(PO_4)_2$) and hydroxyapatite (Hap, $Ca_{10}(PO_4)_6(OH)_2$) are extremely promising due to their outstanding biocompatibility and unique bioactivity, resulting from the high content of this compound in mammalian bones and teeth enamel (Nikpour, 2012).

Hydroxyapatite is one of the most suitable materials for hard tissue engineering applications. The mineral, both pure and in the form of a composite, not only possesses non-inflammatory, non-toxic, and non-immunogenic properties, but is also capable of forming direct bonds with living tissue, as has been proven by numerous researchers (Rupani, 2012; Jin, 2012; Bose, 2012; Ripamonti, 2012). As a result, it can be successfully employed in multiple biomedical applications, such as implant coating, dental filling, orthopedic composites or drug delivery systems. However, pure HAp in the form of powder is regarded as having poor mechanical strength, and therefore cannot be applied in load-bearing situations. Additionally, migration of HAp powder from the implanted site has been observed, which might damage the surrounding healthy tissue (Kong, 2005). These drawbacks can be minimized if the mineral is applied as a filler in a polymer matrix which has the ability to disperse stress, enhance mechanical strength, and at the same time limit the phenomenon of migration.

Few biodegradable polymers are widely used in composite preparation. These are mostly polyesters, for instance poly(lactic acid) (PLA), poly(glycolic acid) (PGA) and their copolymers (PLGA) (Wei, 2004). Chitosan (CS) has already proven to be a particularly good matrix for HAp composite (Peter, 2010; Katti, 2008). CS is a fiber-like biopolymer, which is structurally similar to cellulose and is equally abundant. The polymeric chain of chitosan is composed of D-glucosamine and N-acetyl-D-glucosamine in ß(1-4) linkage. Though chitosan possesses unique properties such as biodegradability, biocompatibility, non-toxicity and antibacterial effect, it does not reflect bone-bonding bioactivity. The bioactive properties of HAp, and the enhancement in mechanical strength of CS, offer new routes for the treatment of damaged hard tissues (Li, 2005). The composite can be prepared in various forms, including porous scaffolds (Kong, 2005), pastes (Murugan, 2004), nanofibers (Zhang, 2008), membranes (Ehrlich, 2006), and implant coatings (Pang, 2005).

During the present research, the mineral composite was prepared with the use of calcium chloride ($CaCl_2$) and disodium hydrogen phosphate (Na_2HPO_4) as sources of calcium and phosphorus, respectively. These reagents are poorly described in the literature as precursors of the mineral phase in CS composite, and therefore the results might be of significant importance.

Materials

Hydroxyapatite (HAp) was precipitated with the use of calcium chloride ($CaCl_2$) and disodium hydrogen phosphate (Na_2HPO_4). Both were purchased from Sigma-Aldrich). Chitosan (CS) was prepared via partial deacetylation of commercially available chitin (Sigma-Aldrich) according to the reaction shown in Fig. 1.
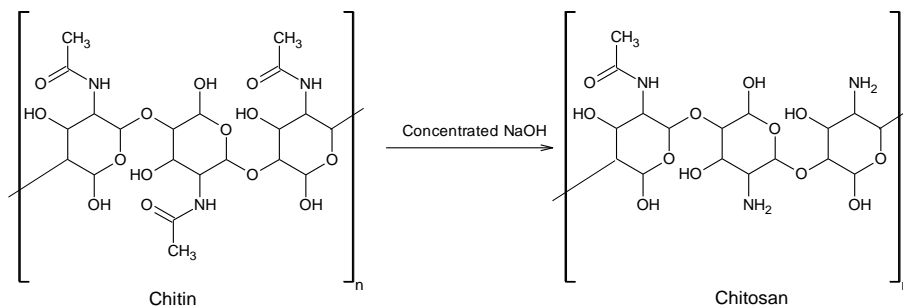
Fig. 1. Reaction of chitin deacetylation to chitosan

Synthesis of hydroxyapatite/chitosan composite via a one-step co-precipitation method

The process of one-step co-precipitation of HAp/CS composite is shown schematically in Fig. 2. A 3% chitosan solution was prepared by dispersing CS powder in a 1% aqueous solution of acetic acid, and stirring until the biopolymer fully dissolved. An appropriate amount of the prepared biomaterial solution was mixed with calcium chloride solution and stirred initially in a three-neck flask. The volumes and concentrations of the $CaCl_2$ and Na_2HPO_4 solutions were taken so as to obtain a final Ca/P ratio of 1.67, which is a characteristic value for HAp present in human hard tissue. The CS solution was introduced into the reactor in such volumes that the weight ratios of the mineral compound to the biopolymer matrix were 85/15, 70/30, 50/50, and 30/70. Na_2HPO_4 was dosed into the mixture, with vigorous stirring, causing the mineral as well as the biopolymer to precipitate gradually. The reaction proceeded in a water bath at a temperature of 40 ^{o}C. When the addition of phosphate was completed, 1M sodium hydroxide solution was added to the mixture dropwise, in order to increase its pH, and causing the CS to fully precipitate. The prepared composite was washed with distilled water, filtered off under reduced pressure, and dried in a convectional dryer at 50 ^{o}C for 24 hours.
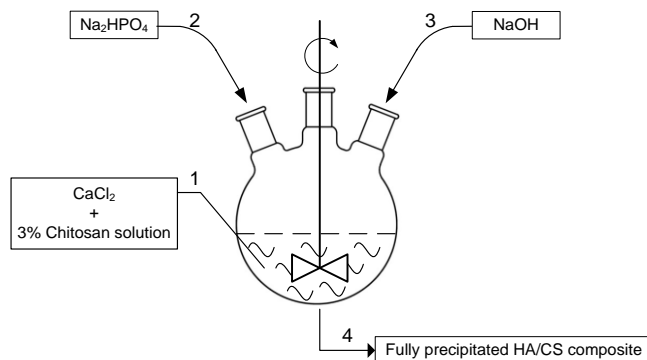

Fig. 2. Schematic diagram of preparation of HAp/CS composite via the one-step co-precipitation method

The product was subjected to numerous analyses. The presence of the expected functional groups was confirmed by FT-IR, recorded on a VERTEX 70 spectrometer (Bruker, Germany). Here the materials were analyzed in the form of tablets, made by pressing a mixture of anhydrous KBr (250 mg) and about 1.5 mg of the tested substance in a special steel ring under a pressure of approximately 10 MPa. The transparent tablet was placed in a cuvette, which was placed in the clamp of the apparatus at the focal point of the beam of radiation. The investigation was performed over a wave number range of 4000–400 cm^{-1} (at a resolution of 0.5 cm^{-1}) with 64 scans.

Samples were also identified using the WAXS (Wide Angle X-Ray Spectroscopy) method, and elaborated with the support of X-RAYAN software. As a result of the analysis, parameters of the crystallographic structure of the composite were obtained.

Thermogravimetric analysis was performed using a Jupiter STA 449 F3 (Netzsch GmbH, Germany) unit in order to record thermal effects during heating. Samples weighing approximately 10.0 mg were placed in an Al_2O_3 crucible, and heated at a rate of 10 ºC/min from 30 ºC to 1000 ºC in a nitrogen atmosphere.

The elemental composition of the biocomposite was determined by means of EDS analysis. Characteristics of the porous structure of selected samples were acquired with use of low-temperature nitrogen sorption, recorded using an ASAP 2020 analyzer (Micromeritics Instrument Co., USA). The BET specific surface area was calculated from the BET equations and the mean pore size (S_p) as well as total pore volume (V_p) were obtained using the BJH algorithm. Description of the morphology of the samples was supported with SEM photographs, recorded from an EVO40 scanning electron microscope (Zeiss, Germany).

Results and discussion

The FT-IR spectra of pure CS and HAp and of composites with various HAp/CS ratios are shown in Fig. 3.

The FT-IR spectrum of pure CS shows a characteristic band around 3430 cm^{-1}, which corresponds to stretching vibrations of hydroxyl groups. Also visible are bands representing the =C=O stretching vibrations and the =N–H in-plane bending vibrations characteristic of amide I and II structures, in the wavelength number range from 1650 to 1600 cm^{-1}. Also a peak characteristic of the amide III structure is visible at 1257 cm^{-1}, whose intensity decreases with increasing HAp content in the composite. Bands visible around 2925 cm^{-1} were attributed to –CH backbone vibrations, while a peak around 1400 cm^{-1} is attributed to –CH$_3$ and –CH$_2$ in-plane deformation vibrations. A series of peaks around 1070 cm^{-1} most likely corresponds to glucosamine stretching vibrations (Zhang, 2011).

The characteristic spectrum of HAp is mainly found at lower wave numbers. Figure 3b shows characteristic bands in the ranges 1150–1000 cm^{-1} and 500–600 cm^{-1}, which can be associated respectively with stretching and bending vibrations of the

PO_4^{3-} group. Also identified are P=O stretching vibrations in the range 1350–1150 cm^{-1}. The peak at 3540 cm^{-1} can be attributed to stretching vibrations of free –OH groups (Danilchenko, 2009; Ehrlich, 2006). The peak is accompanied by a similar one at a lower wave number, which is characteristic of –OH groups subject to intermolecular or intramolecular hydrogen bonds.

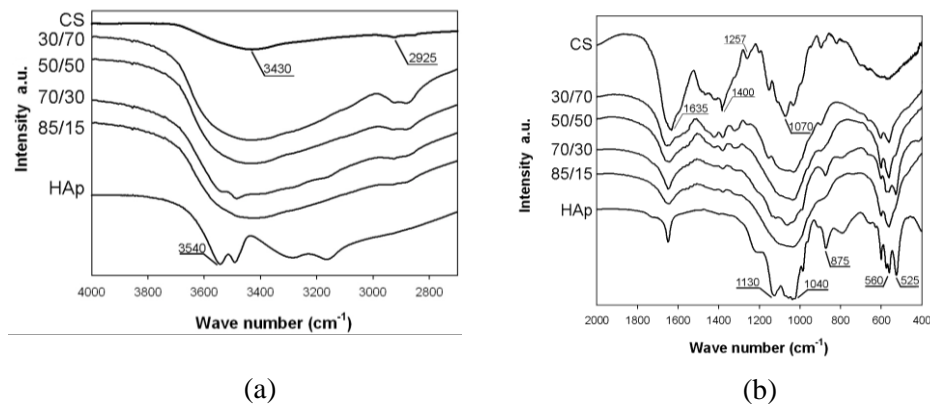(a)   (b)

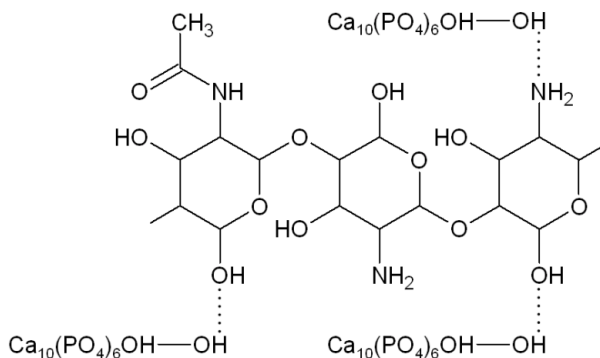Fig. 3. Comparison of FT-IR spectra of pure CS, HAp, and HAp/CS composites with various component ratios

Fig. 4. Schematic representation of hydrogen bonds between HAp and CS compounds

Comparison of the composites with various HAp/CS ratios reveals some important changes. The peak related to the –CH backbone vibrations of CS clearly decreases in intensity as HAp content increases. Strong deformations of the ß-1,4-glycosidic linkage throughout the composite setup, represented by the peak with maximum at 896 cm^{-1}, are confirmations of hydrogen interactions between HAp and CS. The disappearance/deformation of the ether bond in the pyranose ring at 1153 cm^{-1} and the amide III band at 1257 cm^{-1} serves as additional evidence for the chemical interconnection of the two phases. Moreover, the peaks attributed to stretching

vibrations of hydroxyl groups show a slight shift towards lower wavenumbers. For pure HAp the peak was recorded at 3540 cm^{-1}, while for composites it appeared at 3430 cm^{-1}. The slightly lower values of the peak for composites most likely indicate the formation of hydrogen bonds between compounds of the mineral and the biopolymer, shown schematically in Fig. 4.

X-ray diffraction patterns of the obtained composites are shown in Fig. 5. For a pure HAp sample, the existence of 2θ peaks at approximately 26.0^o, 31.4^o, 32.2^o and 40.1^o was recorded, corresponding to the diffraction planes (002), (211), (300), (310) respectively (data supported by the JCPDS database). The pattern confirms the presence of crystalline HAp obtained via the applied method. Characteristic bands for pure chitosan were located around 25° and can be assigned to chains aligned through intermolecular interactions (Zhang, 2011).
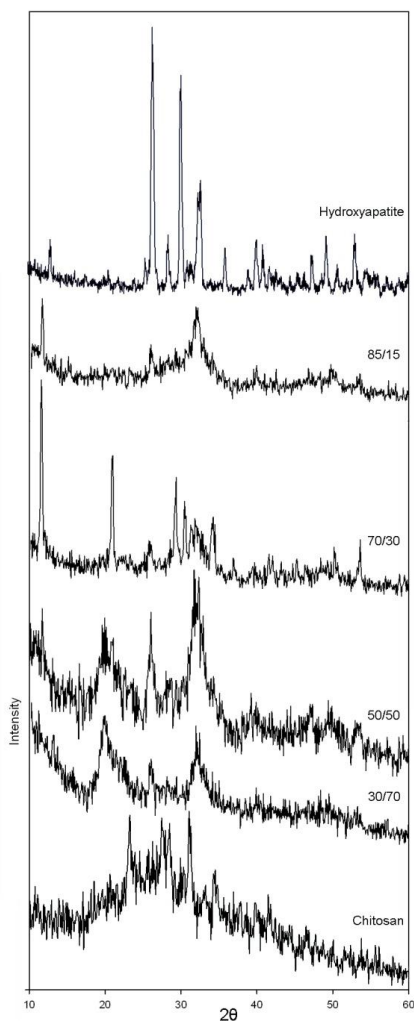
Fig. 5. X-ray diffraction patterns for HAp/CS composites with various ratios

The XRD patterns for the composites suggest that HAp crystallinity decreases with increasing content of the biopolymer. There is a visible broadening of the mineral diffraction peaks with decreasing content of HAp in proportion to chitosan, suggesting diminishing size of the apatite crystals and decrease in its crystallinity (Li 2012, Nikpour 2012). Even for the composite with the lowest content of polymer matrix, it is observable that the crystallization of HAp is already altered. Broadening and weakening of the characteristic peaks of the mineral as well as of the polymer matrix after composite formation indicate bonding of the two phases.
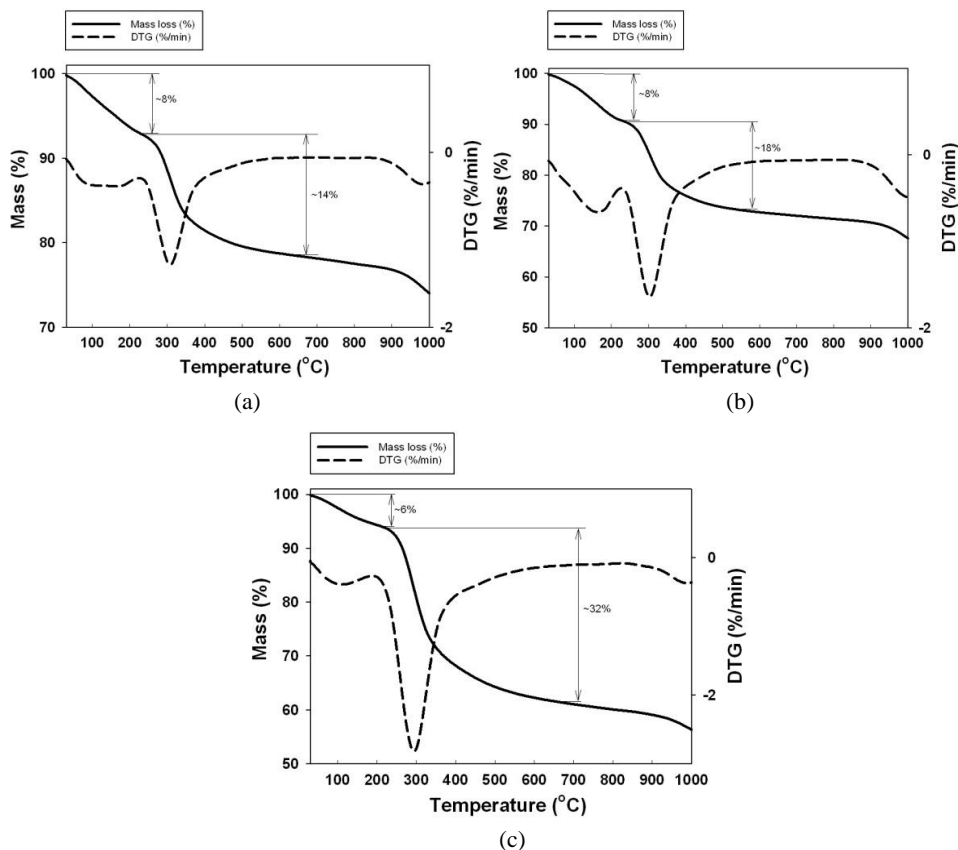

Fig. 6. Thermograms of HAp/CS composites with ratios (a) 85/15, (b) 70/30, and (c) 50/50

In graphs shown as Fig. 6. there are three significant regions visible. The first lies in a temperature range of 100–200 °C, and is most likely connected with the loss of water molecules physically and chemically bound to the CS and HAp. The quantity of water lost ranges from 6% to 8%. The second important mass loss can be observed in the temperature range 200–450 °C, and is attributed to the thermal and oxidative

decomposition of the biopolymer (Neto 2005, Ma 2009). The highest rate of decomposition, represented by the maximum peak of the DTG curve, was found to be around 300 $^{\circ}$C and is constant for all of the tested samples. From the recorded curves it can be noted that the greater the content of organic matrix, the greater the mass loss. For the sample with component ratio 50/50 the mass loss was 32% (Fig. 6c), whereas for the sample HAp/CS 85/15 (Fig. 6a) and HAp/CS 70/30 (Fig. 6b) it was 14% and 18%, respectively. The third characteristic thermal transition, which begins similarly for all samples around 850 $^{\circ}$C, reaches a maximum around 1000 $^{\circ}$C. The peak most likely corresponds to the dehydroxylation stage of the decomposition of HAp. This observation is in agreement with literature data (Wang, 2004).

Energy dispersive spectroscopy (EDS) (Fig. 7) provides important information regarding mineral composition, and can be utilized for determination of calcium and phosphorus content within a specimen. The obtained biomineral ratio of Ca/P was as high as 1.68, which is very close to the molar ratio of the elements in the HAp formula (1.67).

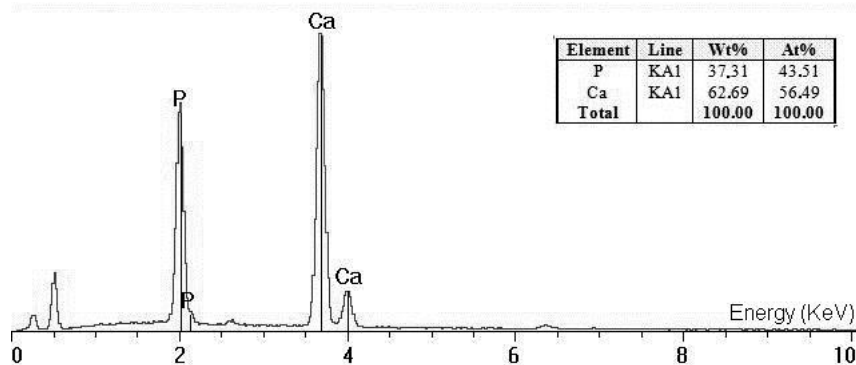| Element	Line	Wt%	At%
P	KA1	37.31	43.51
Ca	KA1	62.69	56.49
Total		100.00	100.00

Fig. 7. EDS spectrum for pure hydroxyapatite, with a Ca/P ratio equal to 1.68

To evaluate the porous structure of the prepared biocomposites, adsorption/desorption isotherms were obtained, which were used to calculate morphological parameters. The results of the analysis are presented in Table 1.

Table 1. Parameters of the porous structure of the prepared composites

Sample name	BET surface area (m^2/g)	Total volume of pores (cm^3/g)	Mean size of pores (nm)
Pure HAp	81.0	0.370	18.2
HAp/CS 85/15	41.0	0.028	2.7
HAp/CS 70/30	23.0	0.016	2.8
HAp/CS 50/50	8.0	0.006	2.8

Values representing the porous structure properties of pure HAp are relatively high, in particular the unusually high total pore volume. The BET surface area for pure HAp is as high as 81.0 m^2/g, the measured pore volume is 0.370 cm^3/g, and the mean pore size is as high as 18.2 nm. Such high values most likely result from the crystalline nature of the prepared product. Results from nitrogen adsorption/desorption analysis clearly show a decrease in the specific surface area of the composite with increasing content of the polymer matrix. Among the prepared composites, the highest BET surface area (41.0 m^2/g) was obtained for the sample with the largest fraction of HAp (HAp/CS 85/15). The pore volume for that sample also took a relatively high value (0.028 cm^3/g). For the sample HAp/CS 70/30 a corresponding decrease in morphological parameter values was observed. The BET surface area was 23.0 m^2/g, and the pore volume also diminished, to 0.016 cm^3/g. The sample with the lowest content of mineral phase has the smallest values of BET surface area (8.0 m^2/g) and pore volume (0.006 cm^3/g) among the analyzed samples. The pore size measured for the biocomposites remained at a constant value of approximately 2.8 nm. For the composite HAp/CS 30/70 the porous structure parameters are not presented, because technical difficulties indicating that the obtained results are to be verified by further measurements. The properties of pure CS were similarly difficult to measure. It is easily noticeable that there is a decrease in specific surface area and pore volume with increasing content of organic phase. This observation suggests that the porosity of the biocomposite is mostly associated with the content of HAp in the sample.

The morphological structure of the biocomposite is supported by SEM microphotographs, as presented in Fig. 8. In this image, the plate-like shape of HAp particles incorporated into the CS matrix can be observed. The composite forms non-uniform agglomerates. The structures vary in size from about 500 nm to 5 μm.
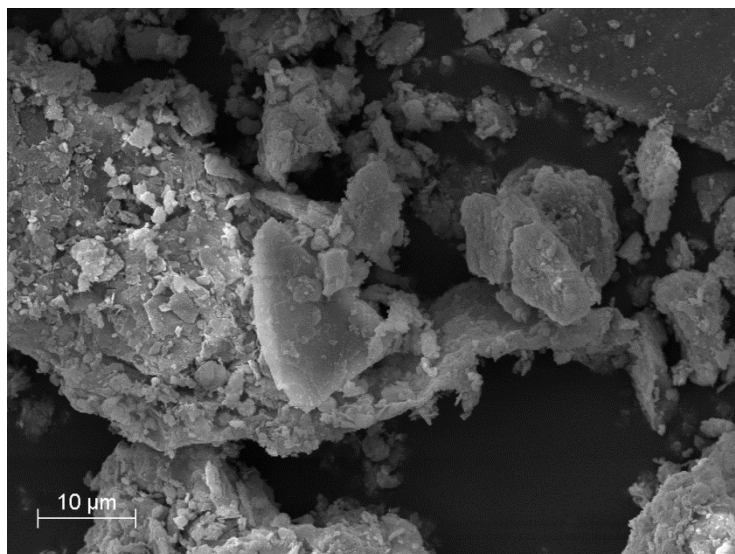
Fig. 8. SEM image of HAp/CS 50/50 composite

Conclusions

As a result of the experiment, HAp/CS composites with various component ratios were prepared via a one-step co-precipitation method, with the use of $CaCl_2$ and Na_2HPO_4 as sources of calcium and phosphorus respectively. CS was obtained through partial deacetylation of commercially available chitin.

The FT-IR spectra of the analyzed samples show that hydrogen bonds formed between the mineral and the biopolymer components, which is confirmed by the shift in the characteristic bands. The analysis provides confirmation of the success of the process of composite synthesis via the selected method. The SEM photographs support the conclusion that the components of the composite are strongly interconnected.

DTG curves show that the prepared composite is thermally stable up to about $200\ ^{o}C$, and two major mass losses are associated with the evaporation of adsorbed water and the degradation of chitosan. Additionally, EDS analysis shows that precipitated HAp has a calcium/phosphorus ratio similar to that of the naturally occurring mineral, thus suggesting that the biomaterial might be suitable for biomedical applications.

The biocomposite with the best morphological properties, namely high specific surface area and porosity, was found to be that with an HAp/CS ratio of 85/15, the highest ratio of mineral to organic phase. With decreasing quantities of porous inorganic mineral, the BET surface area decreases as well. Moreover the pore volume also decreases, suggesting that pores are blocked by the biopolymer.

The experimental results demonstrate the feasibility of preparation of HAp/CS biocomposites using $CaCl_2$ and Na_2HPO_4 via a one-step co-precipitation method.

References

BOSE S., TARAFDER S., 2012, *Calcium phosphate ceramic systems in growth factor and drug delivery for bone tissue engineering: A review*, Acta Biomater., 8, 1401–1421.

DANILCHENKO S. N., KALINKEVICH O. V., POGORELOV M. V., KALINKEVICH A. N., SKLYAR A. M., KALINICHENKO T. G., ILYASHENKO V. Y., STARIKOV V. V., BUMEYSTER V. I., SIKORA V. Z., SUKHODUB L. F., MAMALIS A. G., LAVRYNENKO S. N., RAMSDEN J. J., 2009, *Chitosan–hydroxyapatite composite biomaterials made by a one step co-precipitation method: preparation, characterization and in vivo tests*, J. Biol. Phys. Chem., 9, 119–126.

EHRLICH H., KRAJEWSKA B., HANKE T., BORN R., HEINEMANN S., KNIEB C., WORCH H., 2006, *Chitosan membrane as a template for hydroxyapatite crystal growth in a model dual membrane diffusion system*, J. Membr. Sci., 273, 124–128.

JIN H. H., KIM D. H., KIM T. W., SHIN K. K., JUNG J. S., PARKA H. C., YOON S. Y., 2012, *In vivo evaluation of porous hydroxyapatite/chitosan–alginate composite scaffolds for bone tissue engineering*, Int. J. Biol. Macromol., 51, 1079–1085.

KATTI K. S., KATTI D. R., DASH R., 2008, *Synthesis and characterization of a novel chitosan/montmorillonite/hydroxyapatite nanocomposite for bone tissue engineering*, Biomed. Mat., 3, 034122.

KONG L., GAO Y., CAO W., GONG Y., ZHAO N., ZHANG X., 2005, *Preparation and characterization of nano-hydroxyapatite/chitosan composite scaffolds*, J. Biomed. Mater. Res.; 75A, 275–282.

LI X.Y., NAN K.H., SHI S., CHEN H., 2012, *Preparation and characterization of nano-hydroxyapatite/chitosan cross-linking composite membrane intended for tissue engineering*, Int. J. Biol. Macromol., 50, 43–49.

LI Z., YUBAO L., AIPING Y., XUELIN P., XUEJIANG W., XIANG Z., 2005, *Preparation and in vitro investigation of chitosan/nano-hydroxyapatite composite used as bone substitute materials*, J. Mater. Sci. Mater. Med., 16, 213–219.

NARASARAJU T. S. B., PHEBE D. E., 1996, *Some physico-chemical aspects of hydroxyapatite,* J. Mat. Sci., 31, 1–21.

NETO C.G.T., GIACOMETTI J.A., JOB A.E., FERREIRA F.C., FONSECA J.L.C., PEREIRA M.R., 2005, *Thermal analysis of chitosan based networks*, Carbohydr. Polym., 62, 97–103.

NIKPOUR M.R., RABIEE S.M., JAHANSHAHI M., 2012, *Synthesis and characterization of hydroxyapatite/chitosan nanocomposite materials for medical engineering applications*, Compos.: Part B, 43, 1881–1886.

MA G., YANG D., KENNEDY J. F., NIE J., 2009, *Synthesize and characterization of organic-soluble acylated chitosan*, Carbohydr. Polym., 75, 390–394.

MURUGAN R., RAMAKRISHNA S., 2004, *Bioresorbable composite bone paste using polysaccharide based nano-hydroxyapatite*, Biomat., 25, 3829–835.

PANG X., ZHITOMIRSKY I., 2005, *Electrodeposition of composite hydroxyapatite–chitosan films*, Mater. Chem. Phys., 94, 245–251.

PETER M., BINULAL N. S., SOUMYA S., NAIR S. V., FURUIKE T., TAMURA H., JAYAKUMAR R., 2010, *Nanocomposite scaffolds of bioactive glass ceramic nanoparticles disseminated chitosan matrix for tissue engineering applications,* Carbohydr. Polym., 79, 284–289.

RIPAMONTI U., RODEN L.C., RENTON L.F., 2012, *Osteoinductive hydroxyapatite-coated titanium implants,* Biomater., 33, 3813–3823.

RUPANI A., BASTIDA L.A.H., RUTTEN F., DENT A., TURNER I., CARTMELL S., 2012, *Osteoblast activity on carbonated hydroxyapatite*, J. Biomed. Mater. Res. Part A, 100, 1089–1096.

WANG T., DORNER-REISEL A., MÜLLER E., 2004, *Thermogravimetric and thermokinetic investigation of the dehydroxylation of a hydroxyapatite powder*, J. Eur. Ceram. Soc., 24, 693–698.

WEI G., MA P.X., 2004, *Structure and properties of nano-hydroxyapatite/polymer composite scaffolds for bone tissue engineering*, Biomater., 25, 4749–4757.

ZHANG C. Y., CHEN J., ZHUANG Z., ZHANG T., WANG X. P., FANG Q. F., 2011, *In situ hybridization and characterization of fibrous hydroxyapatite/chitosan nanocomposite*, J. Appl. Polym. Sci., 124, 397–402.

ZHANG Y., VENUGOPAL J. R., EL-TURKIA., RAMAKRISHNA S., SU B., TECK LIM C., 2008, *Electrospun biomimetic nanocomposite nanofibers of hydroxyapatite/chitosan for bone tissue engineering*; Biomater., 29, 4214–4322.